

RESEARCH ARTICLE

Spatial and Temporal Quality of Brain Networks for Different Multi-Echo fMRI Combination Methods

JESPER PILMEYER^{1,2}, GEORGIOS HADJIGEORGIOU^{1,3}, ROLF M. J. N. LAMERICHS^{1,2,4}, MARCEL BREEUWER^{1,5,6}, ALBERT P. ALDENKAMP^{1,7}, AND SVITLANA ZINGER^{1,2}

¹Department of Electrical Engineering, Eindhoven University of Technology, 5612 AE Eindhoven, The Netherlands

²Department of Research and Development, Epilepsy Centre Kempenhaeghe, 5590 AB Heeze, The Netherlands

³Department of Microelectronics, Delft University of Technology, 2628 CD Delft, The Netherlands

⁴Philips Research, 5656 AE Eindhoven, The Netherlands

⁵Department of Biomedical Engineering, Eindhoven University of Technology, 5612 AE Eindhoven, The Netherlands

⁶Philips Healthcare, 5680 PC Eindhoven, The Netherlands

⁷Department of Neurology and Clinical Neurophysiology, Maastricht University Medical Center, 6200 MD Maastricht, The Netherlands

Corresponding author: Jesper Pilmeyer (j.pilmeyer@tue.nl)

This work was supported in part by the Top Consortia for Knowledge and Innovation Public-Private Partnerships (TKI-PPP) under Grant TK11812P07, and in part by the Philips and Eindhoven Engine.


This work involved human subjects or animals in its research. Approval of all ethical and experimental procedures and protocols was granted by the Medical Ethical Committee of the Academic Center for Epilepsy Kempenhaeghe (Heeze, The Netherlands).

ABSTRACT The application of multi-echo functional magnetic resonance imaging (fMRI) studies has considerably increased in the last decade due to superior BOLD sensitivity compared to single-echo fMRI. Various methods have been developed that combine fMRI data derived at different echo times to improve data quality. Here, we evaluated five multi-echo combination schemes: ‘optimal combination’ (OC, T_2^* -weighted), T_2^* -FIT (T_2^* -weighted, calculated per volume), average-weighted (Avg), temporal Signal-to-Noise Ratio (tSNR) weighted, and temporal Contrast-to-Noise Ratio weighted combination. The effect of these combinations, with and without additional postprocessing, on the quality of functional resting-state networks was assessed. Sixteen healthy volunteers were scanned during a 5-minutes resting-state fMRI session. After network extraction, several quality metrics in the temporal and spatial domain were calculated for their respective time-series and spatial maps. Our results showed that OC and T_2^* -FIT outperformed the other methods in both domains. Whereas the OC and T_2^* -FIT time-series were found to be the least associated with artifacts, OC resulted in the highest quality spatial maps. Furthermore, spatial smoothing, bandpass filtering and ICA-AROMA merely improved networks derived from the least performing combinations (Avg and tSNR). Because similar network quality was obtained following OC and T_2^* -FIT without postprocessing, we recommend future studies to implement these combinations without these postprocessing steps. This minimizes the amount of image modifications and processing, potentially leading to enhanced BOLD contrast. The results highlight the benefits of T_2^* -weighted multi-echo combinations on resting-state network quality and raise its potential value in dynamic fMRI analyses or for diagnosis and prognosis purposes of neuropsychiatric disorders.

INDEX TERMS Multi-echo imaging, resting-state, fMRI, brain networks.

I. INTRODUCTION

Over the last decades, functional magnetic resonance imaging (fMRI) has provided numerous novel insights into brain

The associate editor coordinating the review of this manuscript and approving it for publication was Amin Zehtabian .

activation patterns of healthy individuals and patients with neurologic disorders. The application of fMRI has proven to be useful in research domains such as classification of healthy versus diseased individuals [1], the prediction of optimal treatment [2], [3] and the identification of biologically-based subtypes of neurological disorders [4].

Brain networks, commonly called resting-state networks (RSNs), have been widely studied in the healthy population and in neurological disorders for these purposes. For example, the default mode network (DMN), which has been found to be active during self-reflection and inactive during attention-demanding tasks [5], can be robustly detected during resting-state fMRI and abnormal activity of this network has been linked with major depressive disorder [6], [7], [8]. Other consistently identified RSNs are the executive control network (ECN) and the salience network (SN) [6], [8], [9], [10].

In standard (i.e. single-echo) fMRI, a single slice is acquired after each radiofrequency (RF) excitation pulse at a specific echo time (TE) [11]. Despite its non-invasiveness and high spatial resolution, single-echo fMRI is prone to different noise sources that can be of physiological, motion, thermal or hardware-related origin [12]. To increase the sensitivity of the acquired blood oxygenation level-dependent (BOLD) contrast in fMRI and to reduce signal dropout, an MRI technique called multi-echo (ME-)fMRI has been developed [13], [14]. In ME-fMRI, slices are acquired at different TE s following each RF-pulse [11]. Signals acquired at shorter TE s have higher signal intensity than longer TE s [11]. However, the contrast between gray and white matter (GM; WM) and cerebral spinal fluid (CSF) has been shown to be higher at longer TE s [11]. Thus, by combining the images that are acquired at different TE s, an optimal balance between signal intensity and tissue contrast can be obtained, thereby increasing the sensitivity of the BOLD contrast. Several of such multi-echo combination methods have been developed. Examples are the temporal Signal-to-Noise Ratio (tSNR) combination [15] and a T_2^* -weighted combination (also called 'optimally combined', OC) [13], the latter takes into account the variation of T_2^* – known to be dependent on the brain location and tissue type [16] – over the brain.

There is a scarcity of studies investigating the effect of the different ME combination methods on fMRI data [15], [17], [18], [19]. For example, a previous study compared the BOLD sensitivity of multi-echo fMRI data after combination of a simple echo summation scheme, a temporal Contrast-to-Noise Ratio (tCNR) weighted combination or the OC combination to data acquired by single-echo fMRI [18]. They found significant sensitivity increases of more than 7% and 11% for the OC and tCNR-weighted combination method, respectively. Larger increases were found in regions with a short or long T_2^* that are more susceptible to signal dropout in single-echo fMRI [18]. A different study assessed the tSNR, functional connectivity and RSN correlation and size for a single-echo, and OC with or without denoising acquisitions. They found increased values for all measures in OC compared to a single-echo and in OC with denoising compared to OC without denoising [19]. Another recent study showed that the T_2^* -weighted and the tCNR-weighted combination methods increased the tSNR of resting-state fMRI time-series by more than 30% over the

whole brain compared to single-echo [17]. Controversially, results from a dual-echo study indicated that there were no significant sensitivity advantages on a group-level by using tSNR-weighted or tCNR-weighted multi-echo combination over simple multi-echo averaging [15].

Thus, whereas the majority of studies in general show that tCNR and OC increase fMRI data quality compared to single-echo or multi-echo data combined using simple echo summation or tSNR weights, there are also discrepant findings. Whether tCNR or T_2^* -weighted combinations should be used in future studies is still up for debate and remains a rather arbitrary decision. In addition, the effect that echo combination schemes and denoising approaches have on RSN quality has not been studied before. Insights on this topic could support researchers in making more objective decisions regarding multi-echo fMRI processing prior to brain network analyses.

Hence, in the current paper, the effect of different echo combinations, with or without additional postprocessing, on resting-state networks is evaluated. In our approach, five different echo combination methods will be applied to multi-echo resting-state fMRI data: Average (Avg), tSNR, tCNR, OC and T_2^* -FIT (T_2^* -weighted, weights calculated per volume) echo combination. The temporal and spatial quality measures between resting-state networks resulting from the different echo combinations will be compared between each other and between the second echo (SE) reference. Based on previous work we expect enhanced temporal and spatial quality of RSNs for the tCNR, OC and T_2^* -FIT combination compared to the SE and Avg reference. Additionally, we hypothesize that the T_2^* -weighted combinations (OC and T_2^* -FIT) improve the temporal or spatial properties of the RSNs compared to the other multi-echo methods as a result of the echo weight optimization based on the T_2^* estimation per voxel.

The contributions of this study are as follows. First, our study sheds light on the currently unknown effects of different echo combination methods on RSNs. This is essential because future ME studies could benefit from improved brain network maps and time-series. Second, based on our analysis regarding the effect of several pre-processing methods on RSNs, other researchers might opt to adjust their fMRI processing pipeline to further optimize the quality of networks. Consequently, the reliability of results from studies that assess the functioning of the brain enhances. Ultimately, this contributes to the understanding of brain disorders and development of more objective diagnosis and prognosis thereof.

II. MATERIALS AND METHODS

The following subsections describe the main steps from the acquisition of the MRI data up until the evaluation of the consistency metrics between different echo combination methods. Fig. 1 shows a schematic of these analysis steps required to obtain the final results.

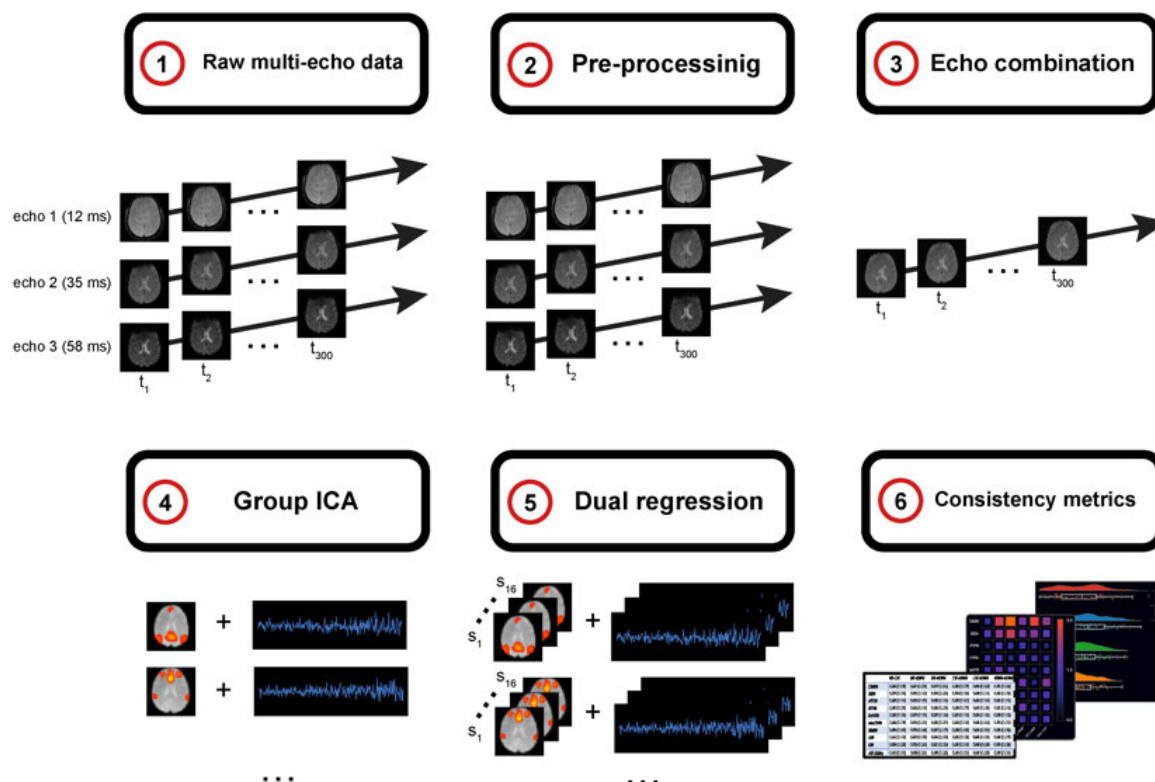


FIGURE 1. Schematic of the required analysis steps to obtain the consistency metrics between resting-state networks. 1) The raw data are the multi-echo data, i.e. three time-series acquired at different echo times. 2) Pre-processing steps are applied. 3) The three time-series are combined using the different combination methods, resulting in a single combined time-series. For the single-echo reference, the second echo time-series is taken. 4) Group independent component analysis (ICA) results in groupwise spatial maps and time-series. 5) Individual spatial maps and time-series are obtained from dual regression. 6) The resting-state networks of all subjects and combination methods are evaluated for temporal and spatial differences.

A. PARTICIPANTS

Sixteen healthy subjects participated in this research and all of them gave informed consent. None of the subjects had a medical history of neurologic or psychiatric disorders and they were between 20-65 years old (age = 43.4 ± 12.7 years old, 11 females and 5 males). The study was approved by the Academic Center for Epilepsy Kempenhaeghe (Heeze, the Netherlands) based on METC approval N16.098.

B. DATA ACQUISITION

Scanning was performed on a Philips Achieva MRI scanner (3 Tesla). At first, a T1-weighted anatomical scan was recorded using a 3D spoiled gradient-echo sequence (repetition time (TR) = 8.3 ms, TE = 3.5 ms) resulting in a matrix size of $240 \times 240 \times 180$ with isotropic voxels of 1 mm. ME (3 echoes) images (300 volumes per echo) were acquired using a gradient-echo EPI sequence (TR = 2000 ms, TE = 12 ms, echo spacing = 23 ms, flip angle = 90° , acquisition bandwidth = 4298 Hz/pixel). In total, 26 slices with a slice thickness of 4.5 mm (no gap) were obtained with an in-plane resolution of 3.5 mm x 3.5 mm and a final in-plane resolution of 3.5 mm x 3.5 mm. A SENSE acceleration factor of 2.7 was applied in the read-out direction.

C. IMAGE PRE-PROCESSING

The fMRI images were slice timing corrected using the Statistical Parametric Mapping (SPM) toolbox, version 12 (<https://www.fil.ion.ucl.ac.uk/spm/software/spm12>) [20], implemented in MATLAB version R2019a (MathWorks). The toolbox MCFLIRT from the FMRIB Software Library (FSL) 6 package was used to estimate the realignment parameters of the volumes to the reference image [21]. The reference image was chosen to be the first image of the second echo due to its echo time being closer to the brain's average T_2^* time. The estimated realignment parameters resulting from echo 2 were applied to echo 1 and 3 using FSL's FLIRT. After these minimal processing steps, the echoes were combined using the different combination schemes as described in the next subsection 'D. Multi-echo combination methods' in a custom MATLAB script (MATLAB version R2019a, MathWorks). Subsequently, the T1-weighted image was coregistered to the functional reference image using a 6 degrees-of-freedom transformation, estimated based on normalized mutual information. The T1-weighted images were then intensity non-uniformity corrected and segmented into CSF, WM and GM, followed by normalization of the coregistered anatomical and functional images to MNI space

by applying a 12 degrees-of-freedom transformation using SPM12.

In standard research practice, additional denoising methods such as bandpass filtering or smoothing are applied to further clean the BOLD signal. However, it has been shown before that these steps may not be necessary or can even decrease effect sizes following ME combination and cleaning [22]. To date, the effect of additional denoising on the quality of resting-state networks is still unknown. Therefore, the temporal and spatial quality measures of the resting-state networks were assessed for the following three cases:

1. No additional denoising.
2. Minimal smoothing with a Gaussian filter with a full width at half maximum of 5 mm [23] and bandpass filtering between 0.05 and 0.2 Hz. Conservative smoothing and bandpass filtering were applied to ensure these postprocessing steps did not completely obscure the effect of ME combination. The bandpass cutoff frequencies were chosen to remove the most common fMRI artifacts: the 0.2 – 0.25 Hz range is linked with contamination of respiratory signals while the 0 – 0.05 Hz is frequently obscured by scanner drift (0 – 0.01 Hz) and respiration-induced CO2 fluctuations (0 – 0.05 Hz) [12].
3. Smoothing as described above, followed by automated ICA-based cleaning using ICA-based Automatic Removal Of Motion Artifacts (ICA-AROMA) [24] to reduce motion artifacts. Subsequently, the time-series were bandpass filtered as described above. This order of denoising steps was recommended in ICA-AROMA’s manual.

D. MULTI-ECHO COMBINATION METHODS

For each described case, the separate echo images were combined according to five different combination schemes below. In addition we used the Avg and SE as reference.

1) OPTIMALLY COMBINED (T_2^* -WEIGHTED)

The OC combination method was developed by Posse et al. [13] and is the combination scheme implemented in the ME denoising method ME-ICA by Kundu et al. [25]. The OC algorithm optimizes contrast by estimation of T_2^* for each voxel [13], leading to reduction of susceptibility artifacts and thermal noise [26]. The weights for echo combination are calculated as follows:

$$w_{n,OC} = \frac{TE_n \cdot e^{-\frac{TE_n}{T_2^*}}}{\sum_{i=1}^3 TE_i \cdot e^{-\frac{TE_i}{T_2^*}}} \quad (1)$$

where TE is the echo time and T_2^* is the estimated T_2^* from each voxel, and the indices n and i relate to the echo number. After calculating the weights for all three echo images, the combined fMRI time-series of each voxel can be calculated by taking the weighted average using the optimally combined weights.

2) T_2^* -FIT (T_2^* -WEIGHTED)

The weights of the T_2^* -FIT method as described by Heunis et al. [17] are also calculated from Equation 1. The T_2^* values and weights, however, are estimated per volume instead of over the whole time-series, i.e. not only each echo will have a different weight but also each volume.

3) tSNR-WEIGHTED

In the tSNR-weighted echo combination method, first the tSNR of every voxel’s time-series of each echo image is calculated. The tSNR is defined as the mean time-series divided by its standard deviation. Subsequently, the following equation can be used to calculate the weight, w_n , tSNR, of the image with echo n [15]:

$$w_{n,tSNR} = \frac{tSNR_n}{\sum_{i=1}^3 tSNR_i} \quad (2)$$

where $tSNR_n$ is the temporal signal-to-noise ratio of the image with echo n , and i the echo index used to sum over all three echo images. After calculating the weights for all three echo images, the combined fMRI time-series of each voxel can be calculated by taking the weighted average using the tSNR-based weights.

4) tCNR-WEIGHTED

The tCNR-weighted echo combination approach, introduced by Poser et al. [18], combines the TE and tSNR values for each echo image reflecting the temporal contrast-to-noise ratio of the images. The advantage of this method is that it does not make any assumptions about the signal and noise because it is measured from the data while it simultaneously incorporates the echo time simultaneously. The tCNR weights are calculated as follows:

$$w_{n,tCNR} = \frac{tSNR_n \cdot TE_n}{\sum_{i=1}^3 tSNR_i \cdot TE_i} \quad (3)$$

Again, the weighted average is calculated to retrieve the final tCNR-weighted combined fMRI image.

5) AVERAGE REFERENCE

To compare the RSNs of ME combinations to a simple multi-echo reference, the average of the three echoes was calculated, i.e. three echo weights equal to one third.

6) SECOND ECHO REFERENCE

The RSNs that are extracted from the ME combined scans are compared to those derived from the SE, i.e. single-echo, fMRI images. The TE of the SE images is equal to 35 ms.

E. NETWORK EXTRACTION AND SELECTION

RSNs were extracted by group-level ICA implemented from the Group independent component analysis (ICA) of fMRI Toolbox (GIFT, <http://mialab.mrn.org/software/gift>) [27]. ICA is a widely applied method for blind source separation [28]. By assuming that the data consist of linear

mixtures of unknown independent variables and by maximizing their non-Gaussianity, ICA facilitates the identification of statistically independent components [29]. In fMRI, these components are referred to as the RSNs. In group ICA, first the subjects' fMRI dimensionality was reduced based on a two-stage principal component analysis, followed by extraction of independent components (fast ICA algorithm). The number of components was set to 30 in order to obtain isolated RSNs with minimal contamination from other networks or subdivision into smaller components [30]. This resulted in a spatial map (of z-scores) and time-series for each individual component.

RSNs were identified using a goodness-of-fit approach with the RSN atlas from Smith et al. as [31]. From this atlas, a mask image of each RSN was compared to each of the 30 components. For each component, the network that scored the highest on this goodness-of-fit score was selected. Subsequently, a visual inspection was performed to check the quality of the match. Ultimately, the following eight RSNs were identified: the default mode network (DMN), right and left frontal parietal network (rFPN/IFPN), lateral and medial visual network (latVN/medVN), somatosensory network (SMN), auditory network (AN) and cerebellar network (CN). Fig. 2 shows the identified general resting-state networks [31].

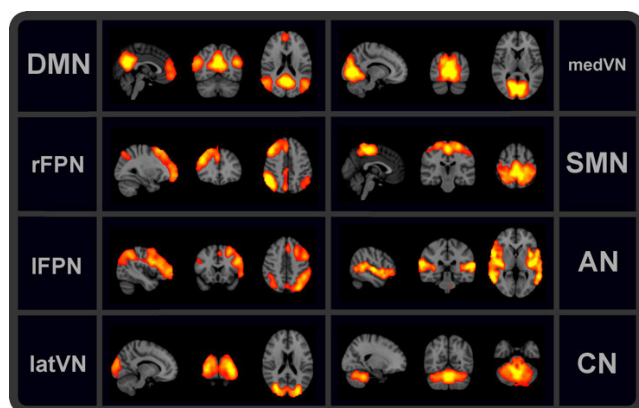


FIGURE 2. Identified resting-state networks. Eight common resting-state networks were identified from the fMRI data following independent component analysis. Abbreviations: DMN = default mode network, rFPN/IFPN = right/left frontoparietal network, lat/medVN = lateral/medial visual network, SMN = sensorimotor network, AN = auditory network, CN = cerebellar network.

F. QUALITY MEASURES

Multiple measures were calculated to compare the properties of the RSNs derived from the combination methods described above. These measures provide insights into the quality of the spatial, i.e. related to the RSN maps, and temporal, i.e. related to the RSN time-series, domain.

1) TEMPORAL MEASURES

The first temporal measure that is implemented is the Pearson correlation of RSN time-series with derived artifact-related

regressors (from here on called *artifact correlation*), which was implemented to assess the networks' extent of temporal confounders such as motion, cardiac and respiratory components. The absolute value of the correlation was calculated to take into account negative and positive correlations. Two motion regressors were derived: framewise displacement (FD) and the derivative of root mean square variance over voxels (DVARS). FD is an indicator of the head movement between subsequent volumes [32] and was calculated from the realignment parameters derived during the realignment step. DVARS reflects the signal intensity changes between subsequent volumes [32]. From the WM and CSF separately, the first five principal components were extracted as implemented in CompCor [33]. Signals from these regions are often assumed to be of non-neural origin, mostly cardiac- or respiratory-related [33]. DVARS and the WM and CSF components were derived from the echo 1 scans as these time-series are not yet ME combined and have the highest signal intensity and therefore assumingly highest artifact content.

The second metric that is calculated is the *dynamic range* (DR) [12], [34]. This feature has been used before to classify independent components as either BOLD or non-BOLD and to estimate the noise contribution in RSNs [34], [35]. Components with higher DR have been associated with true BOLD signals and those with lower DR as noise.

The third temporal metric is the *low to high frequency power ratio* (LHFpow) reflecting the ratio of lower to higher frequencies of which the latter is more often linked to artifact-related power [34]. Similar to DR, components with higher values of LHFpow are associated with RSNs whereas lower ones are more likely to be noise [34]. The DR and LHFpow were both extracted by the GIFT toolbox.

2) SPATIAL MEASURES

The first spatial consistency metric is the Pearson correlation between the identified RSN spatial maps and corresponding RSN spatial maps from the Smith et al. atlas [31] and is referred to as *atlas correlation*. The second metric is the *spatial extent*, i.e. the total number of 'active' voxels. The number of 'active' voxels is defined as the amount of voxels that exceeds a z-score of 3 [36]. In addition, the maximum z-score for each network is obtained and referred to as *spatial stability* [36]. Furthermore, to assess the overall strength of the RSN and ability of group ICA to extract true RSN components, the *mean z-score* is calculated. The spatial extent, spatial stability and mean z-score are calculated for each component after masking each RSN with the corresponding binary RSN of the Smith et al. atlas to avoid the influence of strong noise-related voxels on these metrics [31]. Finally, in order to estimate the ratio between noise and true neuronal signals within each component, the percentage of significant voxels within the CSF and WM to the total number of voxels of that RSN is calculated, referred to as *percentage voxels in CSF & WM*.

3) STATISTICAL ANALYSIS

Distributions of spatial and temporal measures are statistically compared between each combination method and the reference methods (SE and Avg ME combination) using paired t-tests after testing for normality with the Shapiro-Wilk test [37]. p-values (α level = 5%, 1% and 0.1%) are corrected for multiple comparisons using the Holm-Bonferroni procedure [38]. Denoising improvements are compared for each method with respect to the mean improvement of all combination methods by one-sample t-tests. This is done with the aim to evaluate whether and which combination methods benefited significantly more or less from denoising compared to the others. Again, Holm-Bonferroni correction is applied to correct for the numbers of statistical tests. For all t-tests we also ran separate permutation tests to evaluate the validity of the paired t-tests. Permutation tests can be more accurate because there are no distributional assumptions that have to be met and they are an exact approximation of the type I error [39], [40]. We ran a paired sample permutation test based on a t-statistic [41] using a Matlab package [42] and corrected p-values again with Holm-Bonferroni testing. The following settings were used: number of permutations = 5000, tail = two-tailed test and $\alpha = 0.05$. Finally, the observed effect sizes and power for the temporal and spatial measures are calculated and a sensitivity analysis is conducted to identify the smallest detectable effect size with the current study design using the G* Power 3 software package [43].

III. RESULTS

The performance for the combination methods with or without additional denoising is described below. The section is divided into the temporal and spatial domains of the resting-state networks and also a section exploring the network-specific performance. Subsequently, the effect of denoising on the network quality was assessed. The results for the sensitivity analysis for the current study design can be found in Fig. S1. We do not report the permutation test results as the p-values were either highly similar or slightly lower than the paired t-tests, supporting the validity of the latter.

A. TEMPORAL PERFORMANCE

The temporal measures for each combination method are shown in Fig. 3. Improvements in temporal measures versus the reference methods can be found in Fig. S2.

Overall, the time-series of the RSNs from the OC and T_2^* -FIT methods obtained the highest temporal quality measures. Whereas the DR and LHFpow were the highest for T_2^* -FIT (not significant and $p_{\text{corr}} < 0.001$ compared to SE), they also correlated significantly less with the artifact-related time-series compared to Avg ($p_{\text{corr}} < 0.001$). OC resulted in significant improvement compared to Avg in all temporal measures (artifact correlation $p_{\text{corr}} < 0.01$, DR $p_{\text{corr}} < 0.05$ and LTHpow $p_{\text{corr}} < 0.05$). The overall temporal mean observed effect sizes and power ranged from 0.141 to 0.278 and 18.4 to 54.8%, respectively, see Table S1.

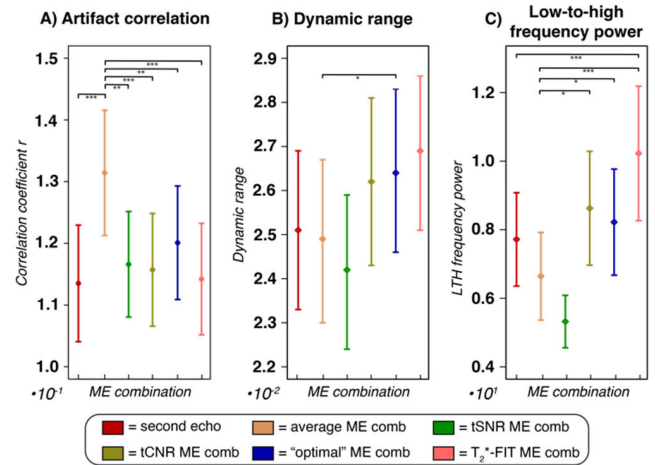


FIGURE 3. A summary of the temporal measures for each multi-echo combination method. T_2^* -FIT showed the highest performance considering all measures. Compared to the other methods, the correlation with artifactual time-series decreased, whereas the dynamic range and low-to-high frequency power increased the most. The mean \pm 95% confidence interval is shown. Statistical significance between the distributions of all combination methods and the second echo or average multi-echo combination were made. Holm-Bonferroni corrected p-values < 0.05 , 0.01 and 0.001 are indicated with *, ** and ***, respectively. Abbreviations: tSNR = temporal signal-to-noise ratio, tCNR = temporal contrast-to-noise ratio, LTH = low-to-high, ME = multi-echo.

To evaluate which nuisance regressors (motion, CSF or WM) were reduced most optimally, the correlation with separate regressors was analyzed. Regarding the motion regressors FD and DVARS, the highest performance was achieved for the tCNR combination (mean $r = 8.82 \times 10^{-2}$), see Fig. S3. For the tissue regressors, the T_2^* -FIT combination correlated the least ($r = 1.18 \times 10^{-1}$).

B. SPATIAL PERFORMANCE

The performance of the combination methods in the spatial domain is shown in Fig. 4. OC combination scored significantly higher on minimal three out of the five spatial measures compared to both reference methods, namely the atlas correlation ($p_{\text{corr}} < 0.001$ vs SE and Avg), spatial extent ($p_{\text{corr}} < 0.01$ vs SE and $p_{\text{corr}} < 0.001$ vs Avg) and mean z-score ($p_{\text{corr}} < 0.001$ vs SE and Avg). Furthermore, compared to Avg, the spatial stability ($p_{\text{corr}} < 0.001$) and percent voxels in CSF & WM ($p_{\text{corr}} < 0.05$) improved significantly. T_2^* -FIT and tCNR also significantly enhanced the spatial quality, with tCNR obtaining the highest spatial stability and T_2^* -FIT the lowest percent voxels in CSF & WM. Overall spatial mean observed effect sizes and power ranged from 0.211 to 0.483 and 35.2 to 95.0%, respectively, see Table S1.

Concluding, OC performed the most optimal. Whereas OC was ranked first on three spatial measures (significantly improved on three spatial measures compared to SE and on all measures compared to Avg), the spatial performance of T_2^* -FIT and tCNR followed.

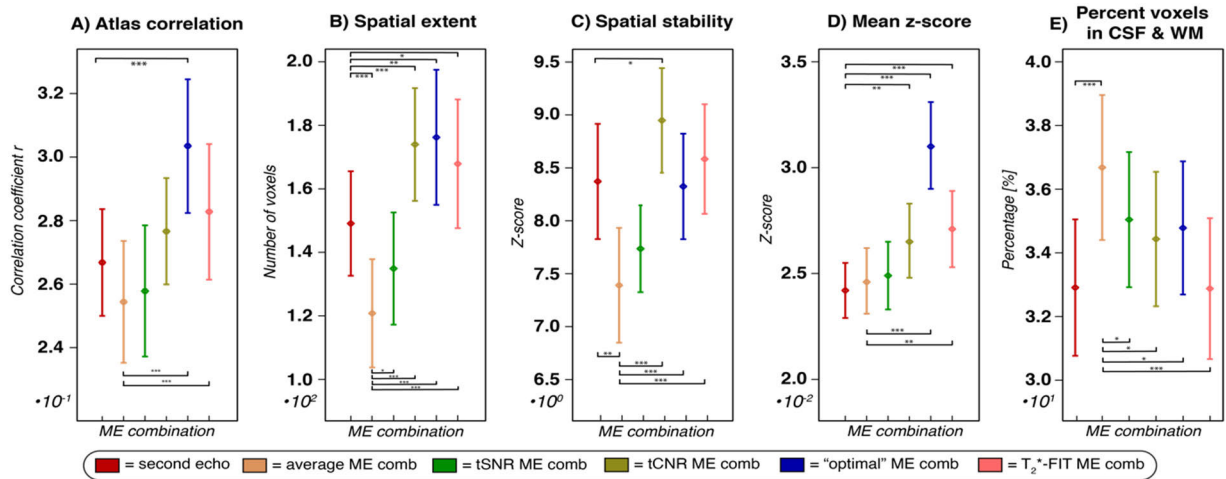


FIGURE 4. A summary of the spatial measures for each multi-echo combination method. Optimal combination performed significantly better than the second echo and average combination on minimal three out of five measures. Moreover, tCNR resulted in the highest spatial stability and T₂*-FIT in the lowest percent voxels in the CSF & WM. The mean ± 95% confidence interval is shown. Statistical significance between the distributions of all combination methods and the second echo or average multi-echo combination were made. The mean ± 95% confidence interval is shown. Statistical significance between the distributions of all combination methods and the second echo or average multi-echo combination were made. Holm-Bonferroni corrected p-values < 0.05, 0.01 and 0.001 are indicated with *, ** and ***, respectively. Abbreviations: tSNR = temporal signal-to-noise ratio, tCNR = temporal contrast-to-noise ratio, CSF = cerebral spinal fluid, WM = white matter, ME = multi-echo.

C. NETWORK-SPECIFIC PERFORMANCE

The improvement of RSN quality resulting from different ME combination methods was assessed at different brain locations: anterior (DMN, IFPN and rFPN), central (SMN and AN) and posterior (CN, medVN and latVN). Fig. 5 displays the improvements of overall RSN quality in these brain areas with regards to the reference methods. Fig. S2 separates the overall quality into temporal and spatial measures. In accordance with previous results, the overall RSN quality improved the most in T₂*-FIT, followed by OC and tCNR.

As expected, the anterior networks gained the most in overall quality for the T₂*-FIT and OC combination. This gain is illustrated best in the spatial domain where both methods improve in quality almost 10% and 30% compared to SE and Avg combination, respectively. The Avg and tSNR combination showed lower performance. For example, the coverage of the lateral prefrontal cortex of the rFPN in the Avg combination was found to be minimal (see Fig. 6), potentially explaining the lower spatial extent and atlas correlation. The tCNR also improved the anterior networks except for the DMN. The spatial map of this network showed that the medial prefrontal cortex region that belongs to the DMN was extended more superior, up until the supplementary motor area, which is not part of the DMN. Compared to SE, the spatial metrics of the anterior networks were less explicitly improved for the OC and T₂*-FIT combination (9% and 10% on average, respectively). Interestingly, the ventromedial prefrontal cortex region in the DMN was smaller for SE and located more distant from the tissue-air boundaries, see Fig. 6.

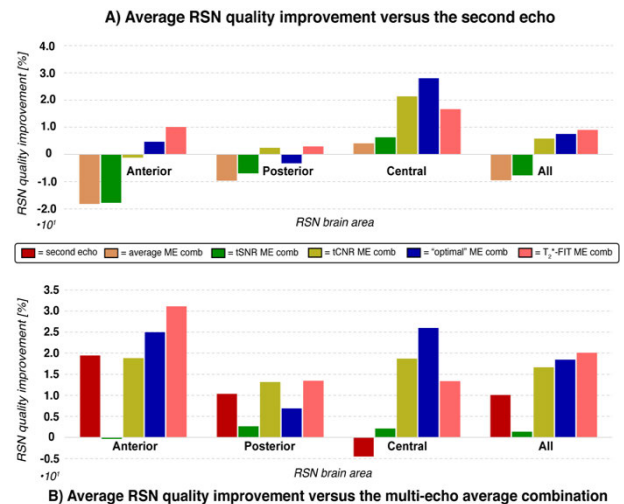


FIGURE 5. Overall quality improvement of anterior, posterior and central brain networks compared to networks from the second echo and average multi-echo combination. Improvements of overall (calculated over the spatial and temporal domain) quality measures of anterior (default mode network, left and right frontoparietal network), posterior (cerebellar network, primary and lateral visual network) and central (sensorimotor network and auditory network) networks are shown, as compared to networks from the second echo (A) and average multi-echo combination (B) references. Note that for the calculations of improvement in artifact correlation and percent voxels in CSF and WM, the sign of change was inverted (as lower artifact correlation and lower percent voxels in CSF and WM correspond to more improvement). Abbreviations: RSN = resting-state network, tSNR = temporal signal-to-noise ratio, tCNR = temporal contrast-to-noise ratio, ME = multi-echo.

For the central (SMN and AN) networks, the difference in performance of the OC and T₂*-FIT versus the reference methods was also substantially larger (on average enhanced

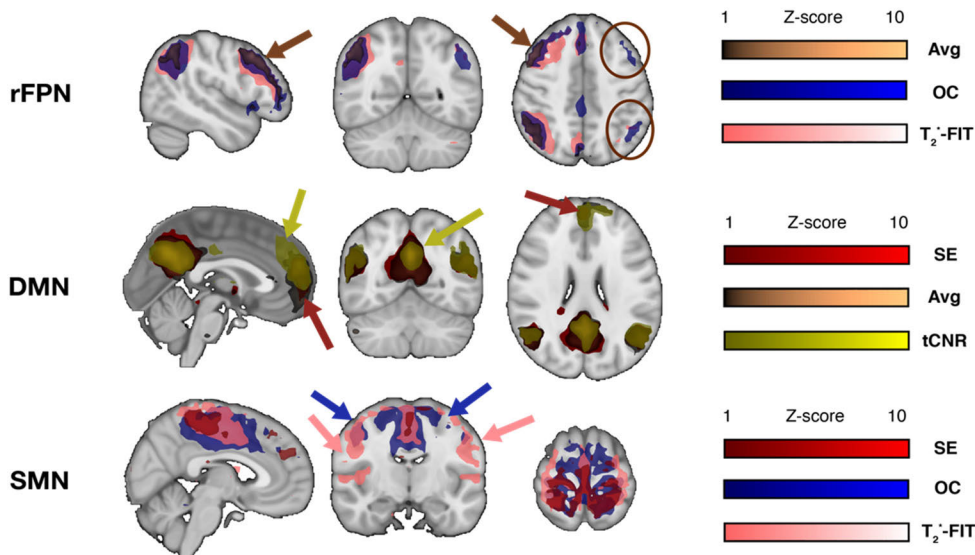


FIGURE 6. Spatial group maps of three resting-state networks. The upper image shows the right frontoparietal network for the Avg, OC and T₂*-FIT combination. For the Avg combination, the coverage of the lateral prefrontal cortex is minimal (brown arrows) and no activation can be seen in the left hemisphere (brown circle). The middle image shows the default mode network for the SE, Avg and tCNR combination. The activation coverage of the brain in the ventromedial prefrontal cortex is relatively small (red arrows) and more distant from tissue-air boundaries for SE. The tCNR combination (yellow arrows) shows limited posterior cingulate cortex activation. Moreover, the anterior activation is shifted towards the supplementary motor area instead of where it is expected to be (medial prefrontal cortex) according to resting-state network atlases. The lower image shows the somatosensory network for SE, OC and T₂*-FIT. The SE network shows small coverage ventrally along the cortex as opposed to OC (blue arrows), and especially T₂*-FIT (pink arrows). Abbreviations: SE = second echo, Avg = average, tCNR = temporal contrast-to-noise ratio, OC = optimally combined, rFPN = right frontoparietal network, DMN = default mode network, SMN = sensorimotor network.

by 28% and 26% for OC and 17% and 13% for T₂*-FIT, for SE and Avg, respectively). The SMN improved most. The spatial map for the SE method showed that the coverage of the SMN was restricted to the superior part of the cortex whereas for the other methods the regions extended also towards the ventral directions along the cortex. The improvement for the posterior networks (CN, medVN, latVN) was less prominent (compared to Avg) or almost nihil (compared to SE).

In the temporal domain, the T₂*-FIT, tCNR and OC combinations also improved the quality of the time-series compared to either the SE or the Avg combination, see Fig. S2. Over all measures and networks, the time-series of the T₂*-FIT method gained the most quality, with an increase of 13% and 25% over the SE and Avg combination, respectively. The largest improvements were observed in the anterior and central brain networks.

D. THE EFFECT OF ADDITIONAL DENOISING

As can be observed from Fig. 7, two combination methods benefited significantly more from smoothing and bandpass filtering in the spatial domain: Avg and tSNR (both p_{corr} < 0.001 compared to the mean improvement). Another remarkable finding is the fact that smoothing and bandpass filtering decreased the quality of the RSN maps of the other methods (p_{corr} < 0.001, < 0.01 and < 0.001 for SE, tCNR and T₂*-FIT, respectively). Other noteworthy effects were a general (i.e. for all combination methods) increasing trend in spatial

extent and decreasing trend in spatial stability. These are likely caused by the smoothing procedure, which could have spread activation patterns and faded activation peaks. Moreover, the percentage of voxels in the CSF and WM was slightly lower for most methods, probably a result of the bandpass filter removing non-BOLD signals in CSF and WM.

Additional ICA-AROMA had only slight effects on the spatial quality. The spatial quality of the tSNR combination decreased whereas the performance of tCNR ‘recovered’.

In the temporal domain, several general trends could be observed for both case 2 and 3. The nuisance correlation decreased by almost 70% for all combination methods, see Fig. S4. This could have been caused by the bandpass filter, potentially removing coherent patterns of artifacts. Because the signal was filtered with a bandpass filter, the dynamic range dropped by about 20 percent for all combination methods. Finally, the LTHpow also dropped by about 40-60%, likely caused by the bandpass filter removing relatively more low frequency power. The differences of decrease in spectral measures and artifact correlation between combination methods, however, was minimal. Nevertheless, a subtle but similar pattern as before was observed for case 2: tSNR benefited the most from smoothing and bandpass filtering (relatively most improvement in DR and LHFpow (p_{corr} < 0.01). Application of additional ICA-AROMA only slightly improved the quality of the RSN time-series for most methods in the spectral domain when compared to no denoising.

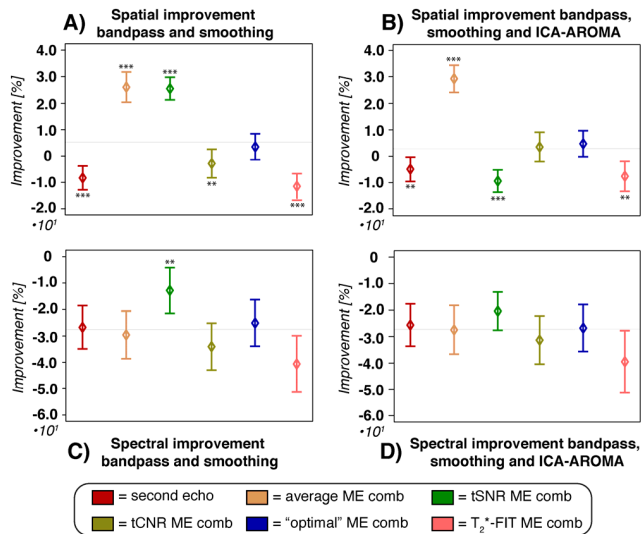


FIGURE 7. The effect of two additional denoising methods on spatial and spectral quality. The upper images show spatial measures changes for each combination method when A) smoothing and bandpass filtering and B) additional ICA-AROMA are applied. The lower images show the spectral measures (dynamic range and low-to-high frequency power) changes when C) smoothing and bandpass filtering and D) additional ICA-AROMA are applied. Statistical testing was performed to test which combination methods improved more than the mean improvement. Holm-Bonferroni corrected p -values < 0.01 and 0.001 are indicated with ** and ***, respectively. The gray line indicates the average improvement. Abbreviations: tSNR = temporal signal-to-noise ratio, tCNR = temporal contrast-to-noise ratio, ME = multi-echo.

IV. DISCUSSION

In this paper we evaluated the quality of the spatial and temporal properties of RSNs between different multi-echo combination methods. Overall, it was shown that the OC and T₂*-FIT combination outperformed the other methods. The OC and T₂*-FIT combination resulted in the highest quality network time-series. The OC combination allowed the extraction of the highest quality spatial maps, followed by T₂*-FIT and tCNR. Compared to SE or the Avg multi-echo combination references, most improvement was observed in the anterior and central networks. Moreover, the effect of denoising on the resting-state networks was assessed. The least performing methods, i.e. the Avg and tSNR combination, benefited the most from additional bandpass filtering and smoothing. These results highlight the strength of T₂*-weighted combination schemes. For T₂*-FIT, OC and tCNR, minimal preprocessing is sufficient to extract robust resting-state networks whereas other methods require additional bandpass filtering and smoothing to obtain comparable network quality.

Compared to OC and tCNR, the T₂*-FIT time-series correlated less with artifact-related time-series and showed lower artifact-related power characteristics. Potentially, the temporally-dependent nature of the T₂*-FIT algorithm, i.e. the estimation of T₂* per volume, could be inherent to this difference in performance. For example, at time points in which noise is more abundant, e.g. during inhalation or head movement, the estimation of T₂* for that voxel may be altered

as a result of the decrease in TE-dependence of the measured signal. Consequently, with T₂*-FIT, more optimal weights can be assigned to the voxel at that time point. For accurate separation of BOLD and non-BOLD components using ICA, this T₂*-based time-varying nature of combining ME data could be fundamental. Note that these results should be interpreted with caution as the effect sizes were just above ($d = 0.278$) what is considered a low effect size [44].

OC outperformed the other methods on spatial quality, followed by T₂*-FIT and tCNR. The increased RSN robustness for OC could be caused by the decreased sensitivity to outliers by the estimation of T₂* over multiple volumes. On the contrary, the OC and tCNR spatial maps contained more voxels within the CSF. The small increase in extent of both OC and tCNR comes at the cost of a percentual increase of non-neural voxels within the spatial maps. Thus, spatial maps derived by T₂*-FIT showed to be still of high quality with minimal overlap of the CSF and WM. Confirmatory, the lower percentage of CSF and WM voxels in the T₂*-FIT networks is also reflected by the temporal measures which indicate less contamination by artifacts (increase in DR and LHFpow and decrease in artifact correlation).

The T₂*-FIT and, especially, OC spatial maps benefited the most from ME, i.e. in comparison to SE, in the anterior networks. One possible explanation is that ME combinations diminish dropout of signals that are prone to susceptibility-related artifacts. Limbic and anterior areas are often affected by signal loss as their T₂* values are reduced from the adjacency to tissue-air boundaries [45], [46]. Indeed, visual inspection indicated that the ventromedial prefrontal cortex cluster of the DMN covered less brain volume closer to the tissue-air boundaries for SE. This difference was subtle compared to T₂*-FIT but more pronounced compared to OC. Another reason could be the fact that the BOLD sensitivity, as observed in the spatial maps, is closer to optimal for T₂*-FIT or OC due to its voxel-specific T₂* estimation. It is known that maximum BOLD sensitivity can be reached if the TE approximates T₂* [11], [47]. The per-voxel estimates of the weights (and thus tuning of the combined echoes and TEs) based on the T₂*-FIT and OC formula take this approximation into account and could underlie the improved spatial quality. Previous research has already shown that T₂* is dependent on the location in the brain [16]. In line with this, OC and T₂*-FIT improved anterior spatial network quality the most out of all methods compared to Avg, suggesting it could be caused by the optimized echo weights and contrast. Thus, the results provide evidence for both, the minimization of signal dropout and the increase in BOLD sensitivity, mostly reflected in the anterior brain area.

The lower tSNR quality metrics might be a result of the way the tSNR-weighting scheme allocates higher weights to earlier echoes. Signal decay increases with TE, i.e. early echoes have significantly higher signal amplitude. The 'noise', or standard deviation of the signal σ , consists of the BOLD fluctuations and non-BOLD noise (including physiological artifacts and thermal 'white' noise). The σ differs

only minimally between echoes compared to the mean of S , making the S/σ weight calculation primarily dependent on the signal S . This causes the combined echo time-series to be heavily weighted towards the early echoes. Moreover, in resting-state fMRI, the BOLD fluctuations are the signals of interest. As the BOLD fluctuations are included in the ‘noise’ σ , i.e. the standard deviation of the signal, in the tSNR formula, echoes with higher fluctuations in BOLD-related signals are penalized. Future studies might opt to recast the formula, e.g. by separating the BOLD fluctuations from the non-BOLD noise by filtering or by substituting the noise components with percent explained variance in the data by nuisance regressors [48]. By using the BOLD fluctuations as signal S and non-BOLD noise as noise σ , the weight calculation takes into account the higher BOLD contrast in the longer TE images. Likewise, in the tCNR-weighted combination, the added TE-factor takes into account the superior BOLD contrast of the longer echoes. The tCNR-weighted combination thus calculates weights that are balanced between signal intensity and BOLD contrast. As our results indicate, networks extracted from tCNR have superior spatial quality compared to tSNR but still lower than the T_2^* -weighted methods (OC and T_2^* -FIT). Moreover, temporal quality metrics (dynamic range and low-to-high frequency power) suggest that the networks from the tSNR combination demonstrate less RSN-related power. This could be a result of the decreased BOLD sensitivity since echoes with a longer TE are weighted less.

Bandpass filtering and smoothing improved the network quality of the Avg and tSNR combinations. Interestingly, these methods showed the lowest performance before additional cleaning. Potentially, these combinations were less efficient at reducing physiological and motion artifacts. The lower performance in the temporal domain supports this hypothesis. For the Avg combination, the artifact correlation revealed the largest abundance of motion, WM and CSF sources in the time-series. tSNR scored the lowest on spectral quality. The fact that the tSNR-combined time-series had the lowest DR and LHFpow of all methods suggests a larger abundance of non-BOLD high-frequency signals. The 0.2 – 0.25 Hz frequency range is associated with contamination of respiratory signals [12]. Bandpass filtering could have reduced the impact of artifact-related signals in the time-series of the Avg- and tSNR-combined networks. Accordingly, the DR and LHFpow of the tSNR-combined time-series relatively improved the most in DR and LHFpow compared to the other methods. More structural removal of these artifacts, e.g. by RETROICOR [49] or ME-ICA [25], [26], or simulations could aid in the process of identifying the origin of this power reduction.

Remarkably, the spatial quality of T_2^* -FIT, tCNR and OC decreased following bandpass filtering and smoothing. Potentially, smoothing decreased the higher BOLD contrast for these combinations. Smoothing usually reduces the randomly distributed noise [11]. However, smoothing of data

with minimal artifacts could reduce the BOLD contrast instead. Moreover, it has already been shown before that smoothing can diminish or abolish ME-based denoising benefits in task-based fMRI [22]. Alternatively, the lowpass cutoff frequency of the bandpass filter at 0.05 Hz could have removed relevant BOLD signals. There is evidence of slow oscillatory (0.01 – 0.05 Hz) signals of neural origin [50], [51], located more significantly in the frontal, parietal and occipital cortices. If artifact-related signals in that frequency range obscured true BOLD signals in the other methods, it could have enhanced performance.

Additional ICA-AROMA did not improve the networks’ spatial and spectral quality for any of the ME combinations in comparison to merely bandpass filtering and smoothing. Yet, there are other ICA-based methods for cleaning the BOLD signal which not have been evaluated here. For example, Tedana [52], a software package that classifies ICA components as BOLD or non-BOLD based on TE dependence regresses out the latter components from the signal to reduce the amount of non-neural contributions. Another common method is ICA-FIX [53], which calculates temporal and spatial measures of the components and classifies them as BOLD and non-BOLD after model training on a by FSL- or user-provided dataset with manually provided labels. The evaluation of the effect of Tedana and ICA-FIX was, however, not performed in this study because Tedana requires multi-echo data and we aimed to also compare the results to SE. ICA-FIX requires the need of a trained dataset and the provided pre-trained dataset has shown inaccurate component classification results and loss of signal [54]. Therefore, we studied the effect of ICA-AROMA, a flexible, easily implemented and well-validated denoising algorithm which has shown to preserve the signal of interest [24], to lead to robust RSN reproducibility while removing noise [54], [55] and increase tSNR [55]. Future studies are required to evaluate whether other ICA-based cleaning methods could lead to further improvements in RSN network quality.

One of the limitations of this study is the small sample size. However, because samples are compared between ME combined datasets from the same participant, i.e. a within-subject design, statistical power increases [56], [57]. The sensitivity analysis showed that true effects of small to medium effect sizes (0.375) could still be detected in this study design with a power of 80%. Observed effect sizes ranged from low to high [44], with the mean effect size of spatial measures being close to medium. The magnitude of the effect sizes for the temporal measures, however, was in the range of what is considered a low effect size [44]. Therefore, a study with more participants is required to confirm these findings. Besides that, more females were scanned than males (approximately a ratio of 2:1). There is evidence of sex differences in RSN connectivity [58], [59]. For example, with increasing age, the central autonomic network has been shown to be functionally altered in females compared to males, reflecting altered autonomic regulation [59]. Another study demonstrated that

the most important contributors to gender prediction based on functional connectivity were connections within the DMN, FPN and SMN [58]. Nonetheless, we analyzed the effects of ME combinations within a participant, thereby reducing the bias of each comparison. Yet, we cannot rule out the existence of a sex*ME combination interaction effect.

In summary, the T_2^* -weighted combinations allowed the extraction of robust and denoised functional maps and time-series of RSNs. Spatial and temporal measures indicated an enhanced performance compared to the reference methods. Moreover, additional denoising, such as spatial smoothing, bandpass filtering and ICA-AROMA, may be unnecessary for the T_2^* -weighted combinations. Consequently, the functional maps remain as intact as possible, whereas smoothing could decrease the BOLD contrast and bandpass filtering could remove low oscillatory neural signals of interest. Studies related to the investigation of the temporal aspects of RSNs might opt to combine ME-fMRI data using the T_2^* -based algorithms. An example of such a study could be the evaluation of RSNs using the wavelet coherence analysis in which phase shifts are a key factor [60]. Artifacts, such as the respiratory artifacts, that are left in the RSN time-series could bias these analyses significantly as these are often emerging as repeating temporal patterns. T_2^* -weighted combinations could decrease the noise correlation and cause a relative power reduction in the high frequency ranges of this physiological confounder. Finally, as bandpass filtering may not be required, potential ultra-low oscillations of neural origin will be left in the BOLD signal.

V. CONCLUSION

The application of multi-echo fMRI in future studies is warranted thanks to its significant increase in BOLD sensitivity when compared to conventional single-echo fMRI. Here, we evaluated the effect of different echo combination methods on the quality of resting-state networks. It was found that the OC and T_2^* -FIT combinations performed better than the second echo and simple multi-echo average weighting scheme. Analyses of network time-series demonstrated that the OC and T_2^* -FIT combination reduced the artifact-related signals most adequately. The OC method demonstrated the most optimal spatial quality measures. Nonetheless, the T_2^* -FIT functional maps still achieved robust and consistently high scores on spatial quality, including the lowest percentage of voxels overlapping with CSF and WM regions. The anterior networks gained the most in overall quality for the T_2^* -weighted echo combinations, potentially reflecting the reduced signal loss in regions that are prone to susceptibility artifacts. Furthermore, additional postprocessing methods to clean the BOLD signal, specifically spatial smoothing, bandpass filtering and ICA-AROMA, were unnecessary for OC and T_2^* -FIT. These T_2^* -weighted combination methods resulted in similar network quality as networks that were derived following other multi-echo combinations and postprocessing steps. Therefore, we recommend future resting-state network studies to apply the OC

and T_2^* -FIT combination without these additional denoising steps. Minimizing the amount of filtering and rescaling of the fMRI images could be beneficial as the original BOLD contrast remains largely untouched. Limitations of the current study include the relatively high repetition time and low sample size. Future studies could examine the effect of T_2^* -based combinations on dynamic network interactions or assess its value in diagnosis or prognosis in populations of specific neuropsychiatric disorders for which fMRI data are still substantially affected by physiological or motion artifacts.

ACKNOWLEDGMENT

The authors would like to thank Dr. Ir. Bernas (Donders Institute for Brain, Cognition and Behavior, Nijmegen, The Netherlands) for their fruitful discussions and for the insights provided by their Ph.D. thesis. It helped them to formulate the research questions, investigated in this paper.

CONFLICTS OF INTEREST

The authors RL and MB are employees at Philips Research (Eindhoven, the Netherlands) and Philips Healthcare (Best, the Netherlands), respectively. The other authors declare that no competing interests exist.

DATA AVAILABILITY

All data that underlie the results are available from: <https://zenodo.org/record/5196276#.YRaHo-2xXyI> (DOI: 10.5281/zenodo.5196276). A preprint of an early version of this paper, which has been modified significantly, can be found at <https://www.biorxiv.org/content/10.1101/2021.08.18.456877v1>.

REFERENCES

- [1] Y. Du, Z. Fu, and V. D. Calhoun, "Classification and prediction of brain disorders using functional connectivity: Promising but challenging," *Frontiers Neurosci.*, vol. 12, p. 525, Aug. 2018, doi: 10.3389/fnins.2018.00525.
- [2] L. M. Jappe, B. Klimes-Dougan, and K. R. Cullen, "Brain imaging and the prediction of treatment outcomes in mood and anxiety disorders," in *Functional Brain Mapping and the Endeavor to Understand the Working Brain*. Rijeka, Croatia: InTech, Jun. 2013, doi: 10.5772/55446.
- [3] S.-G. Kang and S.-E. Cho, "Neuroimaging biomarkers for predicting treatment response and recurrence of major depressive disorder," *Int. J. Mol. Sci.*, vol. 21, no. 6, p. 2148, Mar. 2020. [Online]. Available: <https://pubmed.ncbi.nlm.nih.gov/32245086/>
- [4] A. T. Drysdale, "Resting-state connectivity biomarkers define neurophysiological subtypes of depression," *Nature Med.*, vol. 23, no. 1, pp. 28–38, Jan. 2017, doi: 10.1038/nm.4246.
- [5] J. Posner, J. Cha, Z. Wang, A. Talati, V. Warner, A. Gerber, B. S. Peterson, and M. Weissman, "Increased default mode network connectivity in individuals at high familial risk for depression," *Neuropsychopharmacology*, vol. 41, no. 7, pp. 1759–1767, Jun. 2016, doi: 10.1038/npp.2015.342.
- [6] R. H. Kaiser, J. R. Andrews-Hanna, T. D. Wager, and D. A. Pizzagalli, "Large-scale network dysfunction in major depressive disorder: A meta-analysis of resting-state functional connectivity," *JAMA Psychiatry*, vol. 72, no. 6, pp. 603–611, 2015, doi: 10.1001/jamapsychiatry.2015.0071.
- [7] N. Javaheripour, "Altered resting-state functional connectome in major depressive disorder: A mega-analysis from the PsyMRI consortium," *Transl. Psychiatry*, vol. 11, no. 1, p. 511, Oct. 2021, doi: 10.1038/s41398-021-01619-w.
- [8] C. Zhuo, G. Li, X. Lin, D. Jiang, Y. Xu, H. Tian, W. Wang, and X. Song, "The rise and fall of MRI studies in major depressive disorder," *Transl. Psychiatry*, vol. 9, no. 1, pp. 1–14, Dec. 2019, doi: 10.1038/s41398-019-0680-6.

- [9] P. C. Mulders, P. F. van Eijndhoven, A. H. Schene, C. F. Beckmann, and I. Tendolkar, "Resting-state functional connectivity in major depressive disorder: A review," *Neurosci. Biobehav. Rev.*, vol. 56, pp. 330–344, Sep. 2015, doi: [10.1016/j.neubiorev.2015.07.014](https://doi.org/10.1016/j.neubiorev.2015.07.014).
- [10] Q. Zhao, Z. N. K. Swati, H. Metmer, X. Sang, and J. Lu, "Investigating executive control network and default mode network dysfunction in major depressive disorder," *Neurosci. Lett.*, vol. 701, pp. 154–161, May 2019, doi: [10.1016/j.neulet.2019.02.045](https://doi.org/10.1016/j.neulet.2019.02.045).
- [11] P. Kundu, V. Voon, P. Balchandani, M. V. Lombardo, B. A. Poser, and P. A. Bandettini, "Multi-echo fMRI: A review of applications in fMRI denoising and analysis of BOLD signals," *NeuroImage*, vol. 154, pp. 59–80, Jul. 2017, doi: [10.1016/j.neuroimage.2017.03.033](https://doi.org/10.1016/j.neuroimage.2017.03.033).
- [12] T. T. Liu, "Noise contributions to the fMRI signal: An overview," *NeuroImage*, vol. 143, pp. 141–151, Dec. 2016, doi: [10.1016/j.neuroimage.2016.09.008](https://doi.org/10.1016/j.neuroimage.2016.09.008).
- [13] S. Posse, "Enhancement of BOLD-contrast sensitivity by single-shot multi-echo functional MR imaging," *Magn. Reson. Med.*, vol. 42, no. 1, pp. 87–97, 1999, doi: [10.1002/\(SICI\)1522-2594\(199907\)42:1<87::AID-MRM13>3.0.CO;2-O](https://doi.org/10.1002/(SICI)1522-2594(199907)42:1<87::AID-MRM13>3.0.CO;2-O).
- [14] O. Speck and J. Hennig, "Functional imaging by T_1 - and T_2^* -parameter mapping using multi-image EPI," *Magn. Reson. Med.*, vol. 40, no. 2, pp. 243–248, Aug. 1998, doi: [10.1002/mrm.1910400210](https://doi.org/10.1002/mrm.1910400210).
- [15] Á. Kettinger, C. Hill, Z. Vidnyánszky, C. Windschberger, and Z. Nagy, "Investigating the group-level impact of advanced dual-echo fMRI combinations," *Front Neurosci.*, vol. 10, p. 571, Dec. 2016, doi: [10.3389/fnins.2016.00571](https://doi.org/10.3389/fnins.2016.00571).
- [16] A. M. Peters, M. J. Brookes, F. G. Hoogenraad, P. A. Gowland, S. T. Francis, P. G. Morris, and R. Bowtell, " T_2^* measurements in human brain at 1.5, 3 and 7 T," *Magn. Reson. Imag.*, vol. 25, no. 6, pp. 748–753, Jul. 2007, doi: [10.1016/j.mri.2007.02.014](https://doi.org/10.1016/j.mri.2007.02.014).
- [17] S. Heunis, M. Breeuwer, C. Caballero-Gaudes, L. Hellrung, W. Huijbers, J. F. Jansen, R. Lamerichs, S. Zinger, and A. P. Aldenkamp, "The effects of multi-echo fMRI combination and rapid T_2^* -mapping on offline and real-time BOLD sensitivity," *NeuroImage*, vol. 238, Sep. 2021, Art. no. 118244, doi: [10.1016/j.neuroimage.2021.118244](https://doi.org/10.1016/j.neuroimage.2021.118244).
- [18] B. A. Poser, M. J. Versluis, J. M. Hoogduin, and D. G. Norris, "BOLD contrast sensitivity enhancement and artifact reduction with multiecho EPI: Parallel-acquired inhomogeneity-desensitized fMRI," *Magn. Reson. Med.*, vol. 55, no. 6, pp. 1227–1235, 2006, doi: [10.1002/mrm.20900](https://doi.org/10.1002/mrm.20900).
- [19] A. D. Cohen, A. S. Nencka, R. M. Lebel, and Y. Wang, "Multiband multi-echo imaging of simultaneous oxygenation and flow timeseries for resting state connectivity," *PLoS ONE*, vol. 12, no. 3, Mar. 2017, Art. no. e0169253, doi: [10.1371/journal.pone.0169253](https://doi.org/10.1371/journal.pone.0169253).
- [20] W. Penny, K. Friston, J. Ashburner, S. Kiebel, and T. Nichols, *Statistical Parametric Mapping: The Analysis of Functional Brain Images*. Amsterdam, The Netherlands: Elsevier, 2011. Accessed: Jul. 5, 2022. [Online]. Available: <https://www.elsevier.com/books/statistical-parametric-mapping-the-analysis-of-functional-brain-images/penny/978-0-12-372560-8>
- [21] M. Jenkinson, C. F. Beckmann, T. E. J. Behrens, M. W. Woolrich, and S. M. Smith, "FSL," *NeuroImage*, vol. 62, no. 2, pp. 782–790, Aug. 2012, doi: [10.1016/j.neuroimage.2011.09.015](https://doi.org/10.1016/j.neuroimage.2011.09.015).
- [22] M. V. Lombardo, B. Auyeung, R. J. Holt, J. Waldman, A. N. V. Ruigrok, N. Mooney, E. T. Bullmore, S. Baron-Cohen, and P. Kundu, "Improving effect size estimation and statistical power with multi-echo fMRI and its impact on understanding the neural systems supporting mentalizing," *NeuroImage*, vol. 142, pp. 55–66, Nov. 2016, doi: [10.1016/j.neuroimage.2016.07.022](https://doi.org/10.1016/j.neuroimage.2016.07.022).
- [23] J. Bijsterbosch, S. Smith, S. Forster, O. P. John, and S. J. Bishop, "Resting state correlates of subdimensions of anxious affect," *J. Cognit. Neurosci.*, vol. 26, no. 4, pp. 914–926, Apr. 2014, doi: [10.1162/jocn_a_00512](https://doi.org/10.1162/jocn_a_00512).
- [24] R. H. R. Pruijm, M. Mennes, J. K. Buitelaar, and C. F. Beckmann, "Evaluation of ICA-AROMA and alternative strategies for motion artifact removal in resting state fMRI," *NeuroImage*, vol. 112, pp. 278–287, May 2015, doi: [10.1016/j.neuroimage.2015.02.063](https://doi.org/10.1016/j.neuroimage.2015.02.063).
- [25] P. Kundu, N. D. Brenowitz, V. Voon, Y. Worbe, P. E. Vértes, S. J. Inati, Z. S. Saad, P. A. Bandettini, and E. T. Bullmore, "Integrated strategy for improving functional connectivity mapping using multiecho fMRI," *Proc. Nat. Acad. Sci. USA*, vol. 110, no. 40, pp. 16187–16192, Oct. 2013, doi: [10.1073/pnas.1301725110](https://doi.org/10.1073/pnas.1301725110).
- [26] P. Kundu, S. J. Inati, J. W. Evans, W.-M. Luh, and P. A. Bandettini, "Differentiating BOLD and non-BOLD signals in fMRI time series using multi-echo EPI," *NeuroImage*, vol. 60, no. 3, pp. 1759–1770, Apr. 2012, doi: [10.1016/j.neuroimage.2011.12.028](https://doi.org/10.1016/j.neuroimage.2011.12.028).
- [27] V. D. Calhoun, T. Adali, G. D. Pearlson, and J. J. Pekar, "A method for making group inferences from functional MRI data using independent component analysis," *Hum. Brain Mapping*, vol. 14, no. 3, pp. 140–151, Nov. 2001, doi: [10.1002/hbm.1048](https://doi.org/10.1002/hbm.1048).
- [28] P. Comon, "Independent component analysis, a new concept?" *Signal Process.*, vol. 36, no. 3, pp. 287–314, Apr. 1994, doi: [10.1016/0165-1684\(94\)90029-9](https://doi.org/10.1016/0165-1684(94)90029-9).
- [29] C. F. Beckmann and S. M. Smith, "Probabilistic independent component analysis for functional magnetic resonance imaging," *IEEE Trans. Med. Imag.*, vol. 23, no. 2, pp. 137–152, Feb. 2004, doi: [10.1109/TMI.2003.822821](https://doi.org/10.1109/TMI.2003.822821).
- [30] X. Wang, P. Foryt, R. Ochs, J.-H. Chung, Y. Wu, T. Parrish, and A. B. Ragin, "Abnormalities in resting-state functional connectivity in early human immunodeficiency virus infection," *Brain Connectivity*, vol. 1, no. 3, pp. 207–217, Sep. 2011, doi: [10.1089/brain.2011.0016](https://doi.org/10.1089/brain.2011.0016).
- [31] S. M. Smith, P. T. Fox, K. L. Miller, D. C. Glahn, P. M. Fox, C. E. Mackay, N. Filippini, K. E. Watkins, R. Toro, A. R. Laird, and C. F. Beckmann, "Correspondence of the brain's functional architecture during activation and rest," *Proc. Nat. Acad. Sci. USA*, vol. 106, no. 31, pp. 13040–13045, Aug. 2009, doi: [10.1073/pnas.0905267106](https://doi.org/10.1073/pnas.0905267106).
- [32] J. D. Power, A. Mitra, T. O. Laumann, A. Z. Snyder, B. L. Schlaggar, and S. E. Petersen, "Methods to detect, characterize, and remove motion artifact in resting state fMRI," *NeuroImage*, vol. 84, pp. 320–341, Jan. 2014, doi: [10.1016/j.neuroimage.2013.08.048](https://doi.org/10.1016/j.neuroimage.2013.08.048).
- [33] Y. Behzadi, K. Restom, J. Liu, and T. T. Liu, "A component based noise correction method (CompCor) for BOLD and perfusion based fMRI," *NeuroImage*, vol. 37, no. 1, pp. 90–101, Aug. 2007, doi: [10.1016/j.neuroimage.2007.04.042](https://doi.org/10.1016/j.neuroimage.2007.04.042).
- [34] E. A. Allen, "A baseline for the multivariate comparison of resting-state networks," *Frontiers Syst. Neurosci.*, vol. 5, p. 2, Feb. 2011, doi: [10.3389/fnsys.2011.00002](https://doi.org/10.3389/fnsys.2011.00002).
- [35] S. Robinson, G. Basso, N. Soldati, U. Sailer, J. Jovicich, L. Bruzzone, I. Kryspin-Exner, H. Bauer, and E. Moser, "A resting state network in the motor control circuit of the basal ganglia," *BMC Neurosci.*, vol. 10, no. 1, p. 137, Nov. 2009, doi: [10.1186/1471-2202-10-137](https://doi.org/10.1186/1471-2202-10-137).
- [36] C. Preibisch, J. G. Castrillón G., M. Bührer, and V. Riedl, "Evaluation of multiband EPI acquisitions for resting state fMRI," *PLoS ONE*, vol. 10, no. 9, Sep. 2015, Art. no. e0136961, doi: [10.1371/journal.pone.0136961](https://doi.org/10.1371/journal.pone.0136961).
- [37] S. S. Shapiro and M. B. Wilk, "An analysis of variance test for normality (complete samples)," *Biometrika*, vol. 52, nos. 3–4, pp. 591–611, Dec. 1965, doi: [10.1093/biomet/52.3-4.591](https://doi.org/10.1093/biomet/52.3-4.591).
- [38] S. Holm, "A simple sequentially rejective multiple test procedure," *Scandin. J. Statist.*, vol. 6, no. 2, pp. 65–70, Jan. 1979.
- [39] C. A. Holt and S. P. Sullivan, "Permutation tests for experimental data," *Experim. Econ.*, vol. 26, no. 4, pp. 775–812, Apr. 2023.
- [40] A. Ghasemi and S. Zahediasl, "Normality tests for statistical analysis: A guide for non-statisticians," *Int. J. Endocrinol. Metabolism*, vol. 10, no. 2, pp. 486–489, Dec. 2012, doi: [10.5812/ijem.3505](https://doi.org/10.5812/ijem.3505).
- [41] R. C. Blair and W. Karniski, "An alternative method for significance testing of waveform difference potentials," *Psychophysiology*, vol. 30, no. 5, pp. 518–524, Sep. 1993, doi: [10.1111/j.1469-8986.1993.tb02075.x](https://doi.org/10.1111/j.1469-8986.1993.tb02075.x).
- [42] D. Groppe. (2023). *One Sample/ Paired Samples Permutation t-Test With Correction for Multiple Comparisons*. Accessed: Sep. 14, 2023. [Online]. Available: https://nl.mathworks.com/matlabcentral/fileexchange/29782-mult_comp_perm_t1-data_n_perm-tail-alpha_level-mu-reports-seed_state
- [43] F. Faul, E. Erdfelder, A.-G. Lang, and A. Buchner, "G*power 3: A flexible statistical power analysis program for the social, behavioral, and biomedical sciences," *Behav. Res. Methods*, vol. 39, no. 2, pp. 175–191, May 2007, doi: [10.3758/BF03193146](https://doi.org/10.3758/BF03193146).
- [44] J. Cohen, *Statistical Power Analysis for the Behavioral Sciences*. New York, NY, USA: Academic, 2013.
- [45] D. Cordes, P. A. Turski, and J. A. Sorenson, "Compensation of susceptibility-induced signal loss in echo-planar imaging for functional applications?" *Magn. Reson. Imag.*, vol. 18, no. 9, pp. 1055–1068, Nov. 2000, doi: [10.1016/S0730-725X\(00\)00199-5](https://doi.org/10.1016/S0730-725X(00)00199-5).

- [46] R. Kopietz, J. Albrecht, J. Linn, O. Pollatos, A. Anzinger, T. Wesemann, G. Fesl, T. Stephan, H. Brückmann, and M. Wiesmann, "Echo time dependence of BOLD fMRI studies of the piriform cortex," *Clin. Neuroradiol.*, vol. 19, no. 4, pp. 275–282, Dec. 2009, doi: [10.1007/s00062-009-9010-3](https://doi.org/10.1007/s00062-009-9010-3).
- [47] G. H. Glover, T.-Q. Li, and D. Ress, "Image-based method for retrospective correction of physiological motion effects in fMRI: RETROICOR," *Magn. Reson. Med.*, vol. 44, no. 1, pp. 162–167, 2000, doi: [10.1002/1522-2594\(200007\)44:1<162::AID-MRM23>3.0.CO;2-E](https://doi.org/10.1002/1522-2594(200007)44:1<162::AID-MRM23>3.0.CO;2-E).
- [48] M. Bartoč, R. Mareček, L. Krajčovičová, T. Slavíček, T. Kašpárek, P. Zemánková, P. Říha, and M. Mikl, "Evaluation of different cerebrospinal fluid and white matter fMRI filtering strategies—Quantifying noise removal and neural signal preservation," *Hum. Brain Mapping*, vol. 40, no. 4, pp. 1114–1138, Nov. 2018, doi: [10.1002/hbm.24433](https://doi.org/10.1002/hbm.24433).
- [49] A. T. Baria, M. N. Baliki, T. Parrish, and A. V. Apkarian, "Anatomical and functional assemblies of brain BOLD oscillations," *J. Neurosci.*, vol. 31, no. 21, pp. 7910–7919, May 2011, doi: [10.1523/JNEUROSCI.1296-11.2011](https://doi.org/10.1523/JNEUROSCI.1296-11.2011).
- [50] J. W. Evans, P. Kundu, S. G. Horowitz, and P. A. Bandettini, "Separating slow BOLD from non-BOLD baseline drifts using multi-echo fMRI," *NeuroImage*, vol. 105, pp. 189–197, Jan. 2015, doi: [10.1016/j.neuroimage.2014.10.051](https://doi.org/10.1016/j.neuroimage.2014.10.051).
- [51] J. Bodurka, F. Ye, N. Petridou, K. Murphy, and P. A. Bandettini, "Mapping the MRI voxel volume in which thermal noise matches physiological noise—Implications for fMRI," *NeuroImage*, vol. 34, no. 2, pp. 542–549, Jan. 2007, doi: [10.1016/j.neuroimage.2006.09.039](https://doi.org/10.1016/j.neuroimage.2006.09.039).
- [52] E. DuPre, T. Salo, Z. Ahmed, P. Bandettini, K. Bottenhorn, C. Caballero-Gaudes, L. Dowdle, J. Gonzalez-Castillo, S. Heunis, P. Kundu, A. Laird, R. Markello, C. Markiewicz, S. Moia, I. Staden, J. Teves, E. Uruñuela, M. Vaziri-Pashkam, K. Whitaker, and D. Handwerker, "TE-dependent analysis of multi-echo fMRI with tedana," *J. Open Source Softw.*, vol. 6, no. 66, p. 3669, Oct. 2021, doi: [10.21105/JOSS.03669](https://doi.org/10.21105/JOSS.03669).
- [53] G. Salimi-Khorshidi, G. Douaud, C. F. Beckmann, M. F. Glasser, L. Griffanti, and S. M. Smith, "Automatic denoising of functional MRI data: Combining independent component analysis and hierarchical fusion of classifiers," *NeuroImage*, vol. 90, pp. 449–468, Apr. 2014, doi: [10.1016/j.neuroimage.2013.11.046](https://doi.org/10.1016/j.neuroimage.2013.11.046).
- [54] D. Carone, R. Licenik, S. Suri, L. Griffanti, N. Filippini, and J. Kennedy, "Impact of automated ICA-based denoising of fMRI data in acute stroke patients," *NeuroImage, Clin.*, vol. 16, pp. 23–31, Jan. 2017, doi: [10.1016/j.nicl.2017.06.033](https://doi.org/10.1016/j.nicl.2017.06.033).
- [55] O. Dìpasquale, A. Sethi, M. M. Laganà, F. Baglio, G. Baselli, P. Kundu, N. A. Harrison, and M. Cercignani, "Comparing resting state fMRI de-noising approaches using multi- and single-echo acquisitions," *PLoS ONE*, vol. 12, no. 3, Mar. 2017, Art. no. e0173289, doi: [10.1371/journal.pone.0173289](https://doi.org/10.1371/journal.pone.0173289).
- [56] Y. Guo, H. L. Logan, D. H. Glueck, and K. E. Müller, "Selecting a sample size for studies with repeated measures," *BMC Med. Res. Methodol.*, vol. 13, no. 1, p. 100, Jul. 2013, doi: [10.1186/1471-2288-13-100](https://doi.org/10.1186/1471-2288-13-100).
- [57] D. Lakens, "Calculating and reporting effect sizes to facilitate cumulative science: A practical primer for t-tests and ANOVAs," *Frontiers Psychol.*, vol. 4, p. 863, Nov. 2013, doi: [10.3389/fpsyg.2013.00863](https://doi.org/10.3389/fpsyg.2013.00863).
- [58] C. Zhang, C. C. Dougherty, S. A. Baum, T. White, and A. M. Michael, "Functional connectivity predicts gender: Evidence for gender differences in resting brain connectivity," *Hum. Brain Mapping*, vol. 39, no. 4, pp. 1765–1776, Jan. 2018, doi: [10.1002/hbm.23950](https://doi.org/10.1002/hbm.23950).
- [59] J.-H. Sie, Y.-H. Chen, Y.-H. Shiau, and W.-C. Chu, "Gender- and age-specific differences in resting-state functional connectivity of the central autonomic network in adulthood," *Frontiers Hum. Neurosci.*, vol. 13, p. 369, Oct. 2019, doi: [10.3389/fnhum.2019.00369](https://doi.org/10.3389/fnhum.2019.00369).
- [60] A. Bernas, A. P. Aldenkamp, and S. Zinger, "Wavelet coherence-based classifier: A resting-state functional MRI study on neurodynamics in adolescents with high-functioning autism," *Comput. Methods Programs Biomed.*, vol. 154, pp. 143–151, Feb. 2018, doi: [10.1016/j.cmpb.2017.11.017](https://doi.org/10.1016/j.cmpb.2017.11.017).



JESPER PILMEYER was born in Sittard, The Netherlands, in 1994. He received the B.Sc. and M.Sc. degrees from the Biomedical Engineering Department, Medical Image Analysis Group, Eindhoven University of Technology, Eindhoven, The Netherlands, in 2015 and 2018, respectively, where he is currently pursuing the Ph.D. degree with the Electrical Engineering Department and the Biomedical Diagnostics Laboratory.

The Ph.D. project involves the initiation and completion of a clinical study with the aim of identifying MRI biomarkers for objective depression prognosis. He was with the Epilepsy Centre Kempenhaeghe, as a Software Programmer, to visualize and allow interpretation by clinicians of epileptic spikes in a brain model by clustering dipoles.



GEORGIOS HADJIGEORGIOU was born in Strovolos, Cyprus, in 1996. He received the B.Sc. degree from the Electrical Engineering Department, Eindhoven University of Technology, Eindhoven, The Netherlands, in 2020. He is currently pursuing the M.Sc. degree with the Electrical Engineering Department, Delft University of Technology, Delft, The Netherlands, with a focus on signals and systems.

He was a Software Developer with Adoor. He is also a Product Manager API and Integrations with Worldline.



ROLF M. J. N. LAMERICHS received the M.Sc. degree from the Molecular Sciences Department, Wageningen University, The Netherlands, in 1984, and the Ph.D. degree from Utrecht University, Utrecht, The Netherlands, in 1989, with a focus on the tertiary and quaternary structures of macromolecules and macromolecular complexes determined by multi-dimensional NMR techniques.

After his Ph.D., he joined Philips Healthcare, Best, The Netherlands. He worked on various topics, including the development and evaluation of in-vivo MR spectroscopy methods and exploring the use of MR in molecular imaging. He is currently a Senior Scientist with Philips Research, Eindhoven, The Netherlands. His research interests include functional MRI using state-of-the-art MRI technologies and signal processing methods.



MARCEL BREEUWER was born in The Netherlands, in 1957. He received the M.Sc. degree from the Electrical Engineering Department, Delft University of Technology, Delft, The Netherlands, in 1982, and the Ph.D. degree from Vrije Universiteit, Amsterdam, The Netherlands, in 1985, with a focus on supplementing lipreading with auditory information.

He became a part-time Full Professor of algorithms in clinical image analysis software with the Medical Image Analysis Group, Biomedical Engineering Department, Eindhoven University of Technology, Eindhoven, The Netherlands, where he is currently a part-time Full Professor with the Signal Processing Systems Group, Department of Electrical Engineering. After his Ph.D., he was a Research Scientist and a Senior Scientist with Philips Research, Eindhoven, and Philips Healthcare, Best, The Netherlands, respectively. In 2006, he became a Principal Scientist and the Head of the Cardiovascular Team, Clinical Science and Advanced Development Department, Business Unit Clinical Informatics Solutions. In 2010, he moved to the Clinical Science Department, Business Unit Magnetic Resonance. He is a member of the

Board of the Dutch Society of Pattern Recognition and Image Processing and a fellow of the European Alliance for Medical Engineering Sciences. His research interests include audio, video and medical compression, leading the video coding team and researching the area of image-guided surgery, and medical image processing.



ALBERT P. ALDENKAMP was born in 1951. He received the M.Sc. degree in neuropsychology and the Ph.D. degree in cognition and epilepsy from the University of Groningen, Groningen, The Netherlands, in 1979 and 1984, respectively.

He became a Professor in Leiden and Amsterdam, in 1991 and 1998, respectively. He became the Chair of the Epileptology and Neurocognition, Maastricht University Medical Centre, in 2002.

In addition, he is the Head of the Department of Clinical Neuropsychology and the Vice Chair of the Research Institute of the Tertiary Referral Centre Kempenhaeghe, Heeze, The Netherlands. He is currently a Professor of neuropsychology of epilepsy with the Department of Neurology, Maastricht University Medical Centre, The Netherlands; a Professor of epileptology with the Department of Neurology, Universitair Ziekenhuis Gent, Belgium; and a Professor of imaging in epilepsy with the Department of Electrical Engineering, Eindhoven University of Technology, The Netherlands.

He is a member of six other medical journals, such as *Epilepsy and Behaviour*, *Acta Neurologica Scandinavica*, *Current Neuropharmacology*, *Clinical Neurology and Neurosurgery*, *Current Pediatric Reviews*, and *The Open Pediatric Medicine Journal*. Moreover, he was the Former Secretary of the Commission on European Affairs of the International League Against Epilepsy, and a member of the Dutch Foundation Sepion, the Scientific Committees of Multiple Epilepsy Congresses, the Scientific Committee of the International Bureau for Epilepsy, the International Advisory Board for pharmaceutical companies, the Board of Governors of a Mental Health Institution, and the International Neuropsychology Society. He received the life-time Ambassador of Epileptology Award. He was the Editor-in-Chief of the *Seizure: European Journal of Epileptology*. He is the Co-Editor-in-Chief of the *Journal of NeuroEngineering*.



SVITLANA ZINGER was born in Dnipropetrovsk, Soviet Union, in 1978. She received the M.Sc. degree from the Faculty of Radiophysics, Dnipropetrovsk State University, Dnipropetrovsk, Ukraine, in 2000, specializing in digital signal and image processing, and the Ph.D. degree from the Signal and Image Processing Department, Ecole Nationale supérieure des télécommunications, Paris, France, with a focus on interpolation and resampling of 3D data and its application for urban cartography and for determination of cosmic microwave background, in 2004. In 2005, she was a Postdoctoral Fellow with the Multimedia and Multilingual Knowledge Engineering Laboratory, French Atomic Agency, France, working on the creation of large-scale image ontology for content based image retrieval. From 2006 to 2008, she was a Postdoctoral Researcher with the Center for Language and Cognition, Groningen, The Netherlands, and an Associated Researcher with the Artificial Intelligence Department, University of Groningen, Groningen, working on the retrieval of information from handwritten documents. She is currently an Associate Professor of digital image analysis technologies for healthcare with the Eindhoven University of Technology, Eindhoven, The Netherlands.

...